CrossMark

Artificial neural network modeling of the influence of sol–gel synthesis variables on the photocatalytic activity of TiO$_2$ nanoparticles in the removal of Acid Red 27

**Mohammad A. Behnajady · Hamed Eskandarloo ·
Farzaneh Eskandarloo**

Abstract   In this study, titanium dioxide (TiO$_2$) nanoparticles were prepared by the sol–gel method in different synthesis conditions. The effect of synthesis variables (including water:titanium alkoxide molar ratio, reflux temperature, reflux time, gelation pH, and stirring speed) were studied in the removal of Acid Red 27 as a model contaminant from textile industry under UV light irradiation. For the first time, we report modeling of the effects of synthesis variables on the photocatalytic activity of TiO$_2$ nanoparticles by an artificial neural network (ANN). Five effective synthesis variables were inserted as the input of the network and reaction rate constants (k_{ap}) were introduced as the output of the network. The results showed that the predicted data from the designed ANN model were in good agreement with the experimental data, with a correlation coefficient (R^2) of 0.9655 and mean square error of 0.00148. The designed artificial neural network provided a reliable method for modeling the photocatalytic activity of TiO$_2$ nanoparticles prepared under different synthesis conditions. Furthermore, the relative importance of each synthesis variable was calculated based on the connection weights of ANN model. The reflux time and reflux temperature were the most significant variables in the photocatalytic activity of TiO$_2$ nanoparticles, followed by the water:titanium alkoxide molar ratio and gelation pH.

M. A. Behnajady (✉)
Department of Chemistry, College of Science, Tabriz Branch, Islamic Azad University, Tabriz, Islamic Republic of Iran
e-mail: behnajady@gmail.com; behnajady@iaut.ac.ir

H. Eskandarloo
School of Chemistry, College of Science, University of Tehran, Tehran, Islamic Republic of Iran

F. Eskandarloo
Department of Computer Engineering, Shabestar Branch, Islamic Azad University, Shabestar, Islamic Republic of Iran

🙌 Springer

Introduction

Titanium dioxide is an important semiconductor material, and its applications include sterilization or disinfections [1], gas sensors [2], self-cleaning windows [3], antireflection coatings for photovoltaic cells [4], and photodegradation of organic pollutants in water and air [5]. Titanium dioxide is extensively used as an active semiconductor for photocatalytic reactions because of its availability, nontoxicity, high stability within a wide range of pH, low cost, and a fast electron transfer to molecular oxygen [6]. Titanium dioxide nanoparticles have been prepared by many methods, such as the sol–gel process [7, 8], solvothermal process [9], chemical vapor deposition method [10], electrochemical method [11], reverse micelle method [12], and hydrothermal treatment [13]. The sol–gel process is currently recognized as one of the most widely used techniques for preparing TiO$_2$ photocatalysts because of several advantages, such as low processing temperature, high homogeneity, stability, and versatility of processing [14].

Artificial neural networks (ANN) are the most useful computational tool for many applications, including modeling and simulation [15]. Recently, many researchers have reported the application of ANN for simulating in various fields. For example, Ghanbary et al. [16] applied the ANN technique for modeling the removal of 4-Nitrophenol (4-NP) in different operational conditions (initial nano-TiO$_2$ dosage, irradiation time, UV light intensity, and initial concentration of 4-NP) by the prepared nano-TiO$_2$. By using the ANN model, they have calculated the relative importance of operational parameters on the value of 4-NP removal efficiency. Elmolla et al. [17] employed ANN to predict and simulate COD removal from antibiotic degradation in aqueous solution by the Fenton process. They have reported that the ANN-predicted results were very close to the experimental results. Furthermore, sensitivity analysis showed that all variables under study (reaction time, H$_2$O$_2$/COD molar ratio, H$_2$O$_2$/Fe^{2+} molar ratio, pH, and antibiotics concentration) had a strong effect on antibiotic degradation in terms of COD removal. Khataee and Mirzajani [18] applied the ANN model to predict the photooxidative decolorization of C.I. Basic Blue 3 (BB3), with potassium peroxydisulfate (K$_2$S$_2$O$_8$). Experimental results show that the designed ANN model was successful in predicting the performance of photooxidative decolorization of BB3 solution, and, they also calculated the level of influence of each operational variable (irradiation time, initial concentration of the BB3, initial amount of oxidant, and UV light intensity) on BB3 removal efficiency. Duran et al. [19] applied the ANN technique for modeling the removal of Reactive Blue 4 (RB4) dye from aqueous solution in different operational conditions (initial concentrations of Fe(II), H$_2$O$_2$ and RB4, pH, and temperature) by Fenton reagent under ultraviolet light irradiation. They reported that the designed neural networks were successful in the simulation of the photo-Fenton process for photooxidative degradation of RB4 with

an average error lower than 18 % for the decolorization constant and 14 % for the mineralization constant. A literature review revealed that ANN modeling of the effects of synthesis variables on the photocatalytic activity of TiO$_2$ nanoparticles have not been investigated. The aim of this study was to employ the ANN for modeling of the effects of synthesis variables on the photocatalytic activity of TiO$_2$ nanoparticles in the removal of Acid Red 27 (AR27) for accessing the higher photocatalytic activity. Furthermore, the relative importance of each synthesis variable was calculated based on the connection weights of the ANN model.

Experimental

Materials

The following commercial reagents were used: Titanium tetraisopropoxide (Ti(OC$_3$H$_7$)$_4$), sodium hydroxide (NaOH), nitric acid (HNO$_3$), and methanol (MeOH) with an absolute grade. AR27 which is a monoazo anionic dye was purchased from Merck and used without further purification. The solutions were prepared by dissolving the required quantity of AR27 and synthesized TiO$_2$ photocatalyst in deionized water.

Synthesis method

In our previous work, we reported the preparation of TiO$_2$ photocatalyst by the sol–gel method [20]. To study the effect of synthesis variables, many parameters including reflux time, reflux temperature, gelation pH, water:titanium alkoxide molar ratio, and stirring speed were studied. Initially, titanium precursor (Ti(OC$_3$H$_7$)$_4$) was slowly dissolved in methanol. Then, the obtained solution was sonicated in an ultrasonic bath (Elma, T460/H, 35 kHz, 170 W). The addition of H$_2$O with different molar ratios into a flask containing the solvent–precursor mixture was performed at different reflux temperatures and stirring speeds for various times. The hydrolysis of the alkoxide was carried out at different pH values, adjusted by the addition of sodium hydroxide (NaOH) or nitric acid (HNO$_3$). The obtained sol was dried at 80 °C and finally calcined in air at 450 °C for 3 h. TiO$_2$ nanoparticles prepared in optimal conditions contained mainly anatase phase with particle size in the range of 12–15 nm, band gap energy of 3.28 eV, BET surface area about 99.71 m^2 g^{-1}, and mean pores diameter of 8.7 nm [20].

Photocatalytic activity

The removal of the azo-dye AR27 from aqueous solution was used as a model reaction to evaluate the photocatalytic activity of the prepared TiO$_2$ nanoparticles. Photocatalytic degradation of AR27 was carried out in a batch quartz photoreactor of 100 mL volume with a low-pressure mercury UV-C lamp (15 W; Philips, Netherlands) emitting around 254 nm, in the parallel array, which was placed in front of the quartz tube reactor. The light intensity in the center of the quartz

photoreactor was measured using a Lux-UV–IR meter (Leybold, Germany). The UV irradiation intensity was 56.5 W m^{-2}. In each run, 40 mg of TiO$_2$ nanoparticles were added to 100 mL of the solution and fed into the quartz tube reactor. At given irradiation time intervals, samples (5 mL) were taken out, centrifuged for 10 min (Hettich EBA Centrifuge), and then AR27 concentration was analyzed by UV–Vis spectrophotometer (Pharmacia Biotech Ultrospec 2000) at 522 nm.

Results and discussion

Artificial neural network modeling

An artificial neural networks is a well-known method for its ability in learning, simulation, and prediction of experimental data. A multilayered perceptron (MLP) neural net has an input layer of neuron (independent variables), a number of hidden layers, and the output layer (dependent variables). The number of input and output neurons is determined by the nature of the problem. The hidden layers act like feature detectors; there can be more than one hidden layer [21, 22].

In this study, Matlab mathematical software, 2011 version, was used for ANN calculations. Moreover, a three-layered back-propagation algorithm with tangent sigmoid transfer function (tansig) at hidden layer, and a linear transfer function (purelin) at output layer were designed. The Levenberg–Marquardt back-propagation algorithm was used for training purposes. The input variables of the network were the water:titanium alkoxide molar ratio, reflux temperature, reflux time, gelation pH, and stirring speed, and corresponding reaction rate constants (k_{ap}) were used as output of the network. The ranges of input and output variables are given in Table 1.

The ANN model used experimental datasets in different conditions to test training. In total, 19 tests each with two replicates (38 experimental datasets) were split into training, validation, and test subsets, which contained 18, 9, and 9 datasets, respectively. All inputs and target data must be scaled within a specified range. Therefore, all data (X_i) were scaled (x_i) into the 0.2–0.8 ranges, through Eq. (1) [23, 24];

$$x_i = 0.2 + \frac{0.6(X_i - X_{min})}{(X_{max} - X_{min})} \tag{1}$$

where X_{min} and X_{max} refer to the lowest and the highest value of the input variable X_i, respectively.

The number of neurons in the hidden layer affects the performance of the ANN model. To determine the optimum number of hidden nodes in this study, different numbers of neurons were tested in the range of 1–16, in the hidden layer. Each topology was repeated three times to avoid random correlation due to random initialization of weights. Figure 1 shows the relationship between the mean square error (MSE) and the number of neurons in the hidden layer. As can be seen, the lowest MSE is obtained in about 12 neurons; therefore, 12 neurons were selected for

Table 1 The ranges of input and output variables

Variable	Range
Input layer	
Water:titanium alkoxide molar ratio (mol%)	20–100
Reflux temperature (°C)	50–80
Reflux time (h)	1–6
Gelation pH	3–10
Stirring speed (rpm)	500–1000
Output layer	
k_{ap} (min^{-1})	0.119–0.363

the best performance of the neural network model. Figure 2 shows the schematic illustration of the optimized ANN structure.

Figure 3 shows a comparison between experimental and predicted k_{ap} values for the test set by using the neural network model. The plot in this figure has a correlation coefficient (R^2) of 0.9655. From this plot, it can be seen that the results obtained from the model are in good agreement with the experimental data, and the model can accurately predict reaction rate constants at different synthesis conditions.

Modeling of TiO$_2$ synthesis variables

To study the effect of synthesis conditions in order to achieve TiO$_2$ nanoparticles with high photocatalytic activity, five synthesis variables, including water:titanium alkoxide molar ratio, gelation pH, reflux temperature, reflux time, and stirring speed, were investigated.

The effect of water:titanium alkoxide molar ratio

The semi-logarithmic graphs of the concentration of AR27 in the presence of TiO$_2$ nanoparticles versus irradiation time yielded straight lines with correlation coefficients (R^2) higher than 0.98, indicating pseudo-first-order kinetics. Pseudo-first-order reaction rate constants (k_{ap}) for the removal of AR27 were obtained from the slope of the semi-logarithmic graphs of AR27 concentration versus irradiation time. Figure 4 shows the k_{ap} of AR27 removal by TiO$_2$ nanoparticles calculated by the ANN model and the experimental results as a function of the water:titanium alkoxide molar ratio. The effect of the water:titanium alkoxide molar ratio on the photocatalytic activity of TiO$_2$ was evaluated through preparation of TiO$_2$ nanoparticles in different ratios of H$_2$O in comparison with TTIP: 20:1, 40:1, 65:1, 80:1, and 100:1. It was observed that the photocatalytic activity of the prepared TiO$_2$ nanoparticles significantly increased with increasing H$_2$O/TTIP molar ratio to 65:1. Further increase in the water:titanium alkoxide molar ratio to
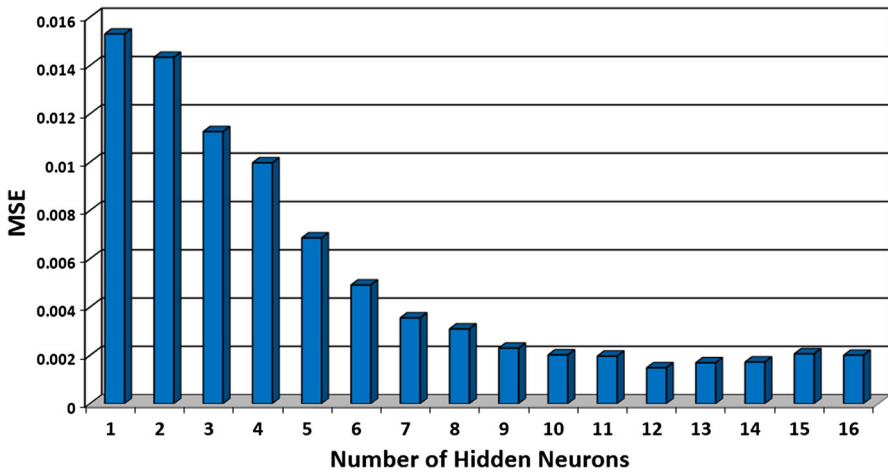
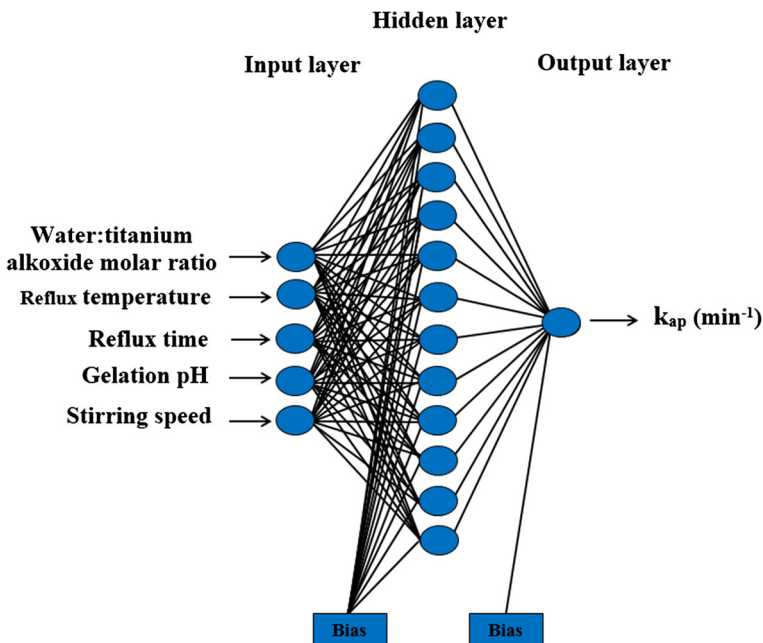**Fig. 1** Effect of the number of neurons in the hidden layer on the performance of the neural network

Fig. 2 Schematic illustration of the optimized ANN structure

more than 65:1 (H_2O/TTIP) decreased the photocatalytic activity. In the presence of higher amounts of water, high hydrolysis rates are desired for the formation of $Ti(OH)_4$ which condenses to yield Ti–O–Ti chains [25, 26]. Thus, the number of active sites can depend on the water amount [25]. The hydrolysis of metal alkoxide
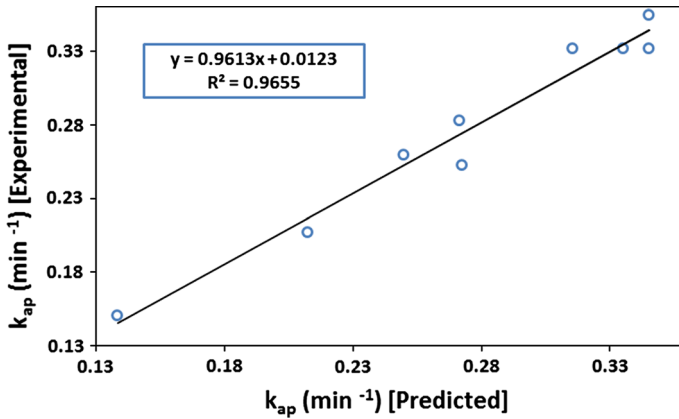
Fig. 3 Comparison between predicted and experimental k_{ap} values for the test set

precursor produces Ti–OH, which can react with an alkoxide molecule or another Ti–OH species or a solvated metal species. The ratio of water to metal alkoxide precursor determines the contribution of each reaction and, consequently, the mechanism of the reaction. The excess water suppresses the development of Ti–O–Ti species, because chemical equilibrium causes favorable creation of Ti–OH species [25, 26]. The results in Fig. 4 show good agreement between the predicted values from the ANN model and the experimental results.

The effect of reflux temperature

To study the effect of reflux temperature on the photocatalytic activity of samples, TiO$_2$ nanoparticles were prepared in three different reflux temperatures of 50, 65, and 80 °C. Figure 5 shows the k_{ap} of the AR27 removal by TiO$_2$ nanoparticles as a function of reflux temperature. The results of the photocatalytic activity show that increasing the reflux temperature from 50 to 80 °C causes an improvement in the photocatalytic activity; this observation shows that the reaction being carried out at the solvent evaporation temperature yields more active nanoparticles than at lower temperatures. The decrease in crystallite size at higher temperatures can be the main cause of improved photocatalytic activity due to higher nucleation rate which has been reported in our previous work [20]. Figure 5 shows that the neural network model correctly predicts k_{ap} of AR27 removal by TiO$_2$ nanoparticles prepared at different reflux temperatures.

The effect of reflux time

The effect of reflux time on photocatalytic activity of TiO$_2$ nanoparticles was investigated in three different reflux times of 1, 3, and 6 h. Figure 6 shows k_{ap} of AR27 removal by TiO$_2$ nanoparticles as a function of reflux time. As can be seen, photocatalytic activity increased with increasing reflux time up to 3 h. This result
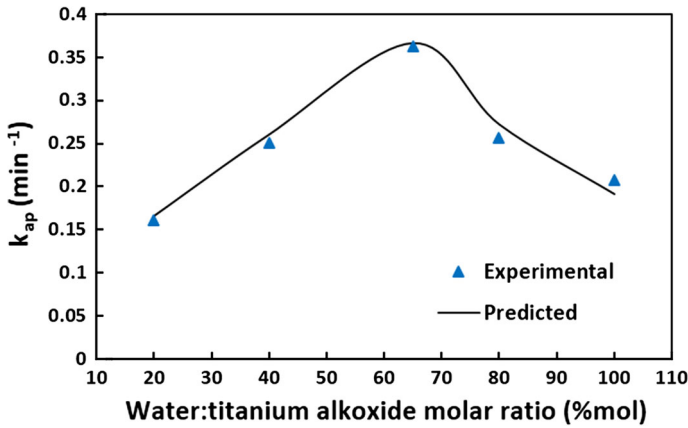
Fig. 4 Comparison between ANN-predicted and experimental values of k_{ap} as a function of the water:titanium alkoxide molar ratio. Reflux temperature = 80 °C, reflux time = 3 h, stirring speed = 1000 rpm, and gelation pH 5
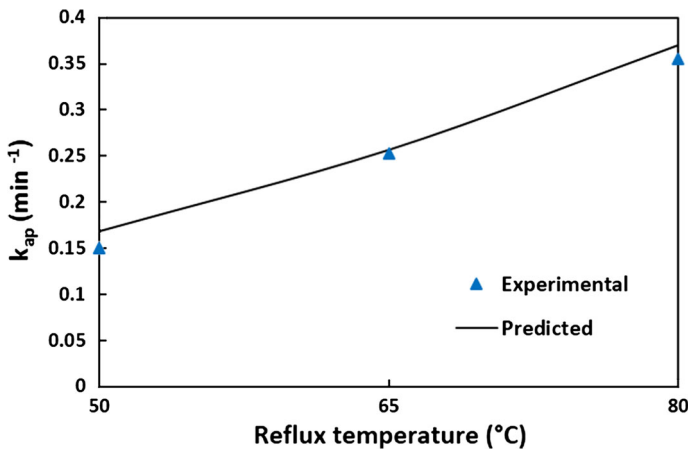

Fig. 5 Comparison between ANN-predicted and experimental values of k_{ap} as a function of reflux temperature. H_2O:TTIP = 65:1, reflux time = 3 h, stirring speed = 1000 rpm, and gelation pH 5

agrees with the findings of Bessekhouad et al. [25], who reported that a 3 h reflux time was enough to produce a catalyst with the highest activity. Bandgar et al. [27] have reported that increasing reflux time causes variation in the crystallite size, band gap energy, and refractive index of TiO_2. Ge et al. [28] have also reported the influence of reflux time (2, 6, and 10 h) on crystallinity, crystal size, and photocatalytic activity of TiO_2 nanoparticles. The highest photocatalytic activity has been reported for the sample prepared under 6 h of reflux time due to proper crystallinity and suitable crystal size. Figure 6 also shows good agreement between the k_{ap} of AR27 removal calculated by the ANN model and the experimental results as a function of reflux time.
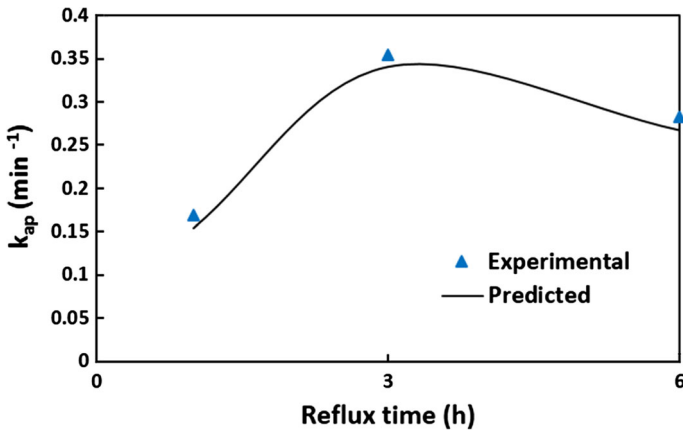
Fig. 6 Comparison between ANN-predicted and experimental values of k_{ap} as a function of reflux time. H$_2$O:TTIP = 65:1, reflux temperature = 80 °C, stirring speed = 1,000 rpm, and gelation pH 5

The effect of gelation pH

Figure 7 shows the k_{ap} of AR27 removal by TiO$_2$ nanoparticles as a function of gelation pH. The effect of gelation pH on photocatalytic activity of TiO$_2$ was evaluated through the hydrolysis of alkoxide at different pH values, adjusted by the addition of sodium hydroxide (NaOH) or nitric acid (HNO$_3$). The results indicate that TiO$_2$ nanoparticles prepared under pH 5 have the highest photocatalytic activity. Barati et al. [29] studied the influence of sol pH on the particle size of TiO$_2$ nanostructures. They reported that, when the pH increases from 4.5 to 7, the particle size of the TiO$_2$ thin film increases. Transformation from Ti(OH)$_4$ to anatase TiO$_2$ and nucleation of anatase are assumed to be inhibited by excessive absorption of hydroxyl ions to TiO$_2$ clusters. Zhang et al. [30] prepared TiO$_2$ nanoparticles using the reverse micelle method under acidic conditions. They found that the concentration of the acid has a major role in the formation of the rutile phase, and higher acid concentration (2.5 M) is better for rutile crystallization. Their product was a mixture of anatase and rutile when the concentration of acid was 2 M. Wei et al. [31] studied the effect of pH in the range of 7–11 on phase content and particle size of TiO$_2$ catalysts. They reported that the presence of a high concentration of hydroxyl ions is more suitable for the formation of the rutile phase. The anatase phase of TiO$_2$ has higher photocatalytic activity in comparison with the rutile phase, because the electron–hole separation in the anatase phase occurs better than in the rutile phase [32, 33]. Therefore, the decrease in the photocatalytic activity in acidic and alkaline circumstances could be due to increasing crystallite size and decreasing anatase phase content of the TiO$_2$ nanoparticles. Figure 7 also shows a comparison between the calculated values from the ANN model and the experimental results of the output variable as a function of gelation pH. The agreement between the values predicted by the model and the experimental results is good.
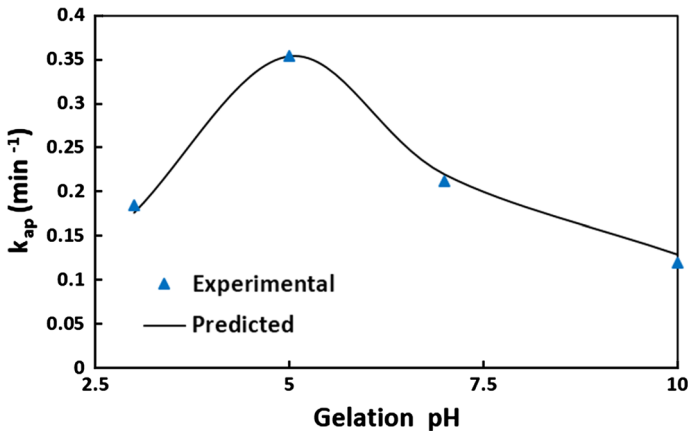
Fig. 7 Comparison between ANN-predicted and experimental values of k_{ap} as a function of gelation pH. H_2O:TTIP = 65:1, reflux temperature = 80 °C, reflux time = 3 h, and stirring speed = 1000 rpm

The effect of stirring speed

To study the effect of the stirring speed of titanium solution on TiO_2 photocatalytic activity, these nanoparticles were prepared in three different stirring speeds of 500, 750, and 1000 rpm. Figure 8 shows the k_{ap} of the AR27 removal by TiO_2 nanoparticles as a function of stirring speed. It was observed that the stirring speed of titanium solution induced the variation of photocatalyst efficiency, and the photocatalytic activity of TiO_2 nanoparticles increased with increasing stirring speed. Panpae et al. [34] studied the influence of stirring speed on the structural properties of nanosized anatase-TiO_2 in the range of 400–1000 rpm. They reported that the intensity of stirring has a significant effect on the final particle size of anatase aggregates and the smallest aggregates (about 6–8 nm) were obtained with a stirrer speed of 1000 rpm. Sathyamoorthy et al. [35] studied the effect of stirrer speed in a range of 200–1200 rpm on the aggregation of anatase TiO_2 nanoparticles. They have reported that, for stirrer speeds over 400 rpm, there is actually a drop in mean aggregate size; due to shear forces beyond a certain stirrer speed, the aggregates simply break into their minimum size. Therefore, increasing photocatalytic activity with increasing stirring speed could be due to the formation of smaller aggregates of TiO_2 nanoparticles. In terms of investigating the relationship between the values calculated by the ANN model and the experimental results, Fig. 8 shows that the predicted values are in good agreement with the experimental results.

ANN model sensitivity analysis

Table 2 shows the weights produced by the ANN model used in this study. The relative importance of each input variable on output variable can be obtained through the neural weight matrix [18, 36, 37].
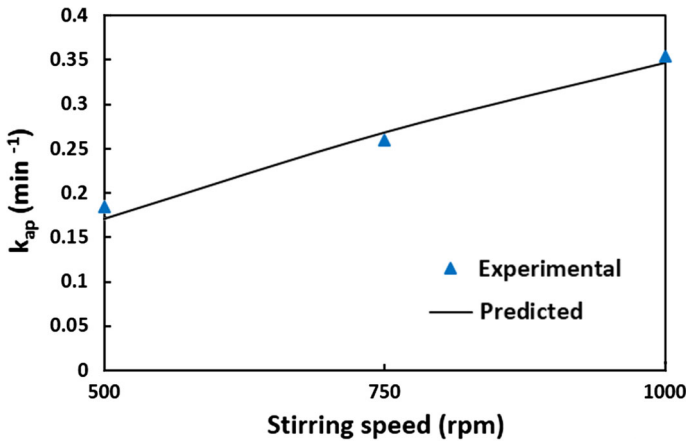
Fig. 8 Comparison between ANN-predicted and experimental values of k_{ap} as a function of stirring speed. H$_2$O:TTIP = 65:1, reflux temperature = 80 °C, reflux time = 3 h, and gelation pH 5

For every input synthesis variable, the percentage change in the output, due to the change in the input variable, was calculated using the following Eq. (2) [23, 36, 37]:

$$I_j = \frac{\sum\limits_{m=1}^{m=N_h}\left(\left(\left|W_{jm}^{ih}\right|\Big/\sum\limits_{k=1}^{N_i}\left|W_{km}^{ih}\right|\right)\times\left|W_{mn}^{ho}\right|\right)}{\sum\limits_{k=1}^{k=N_i}\left\{\sum\limits_{m=1}^{m=N_h}\left(\left|W_{km}^{ih}\right|\Big/\sum\limits_{k=1}^{N_i}\left|W_{km}^{ih}\right|\right)\times W_{mn}^{ho}\right\}} \tag{2}$$

where I_j is the relative importance of the jth input variable on the output variable, and N_i and N_h are the number of inputs and hidden neurons, respectively; W's are connection weights, the superscripts 'i', 'h' and 'o', respectively, refer to input, hidden and output layers; and subscripts 'k', 'm' and 'n', respectively, refer to input, hidden and output neurons.

Figure 9 represents a comparison between the effects of five input synthesis variables as calculated by Eq. (2) on the photocatalytic activity of TiO$_2$ nanoparticles. As Fig. 9 indicates, reflux time and reflux temperature have greater effects on the photocatalytic activity of TiO$_2$, with a relative importance of 35 and 25 %, respectively, followed by water:titanium alkoxide molar ratio and stirring speed.

Conclusions

In this study, the effect of synthesis conditions on the photocatalytic activity of TiO$_2$ nanoparticles prepared by the sol–gel method was modeled with an ANN. A three-layered back-propagation neural network with tansig as transfer function at the hidden layer with 12 neurons was designed to predict the removal of AR27 under different synthesis conditions of TiO$_2$ nanoparticles. The performance of TiO$_2$

Table 2 Weight matrix: weights between input and hidden layers (W_1) and weights between hidden and output layers (W_2)

| W_1							Bias	W_2	
Neuron	Input variable							Neuron	Output
	Reflux temperature	Stirring speed	Reflux time	Gelation pH	Water:titanium alkoxide molar ratio				k_{ap} (min^{-1})
1	-0.145	-1.626	0.879	-1.247	0.458		-2.23	1	-0.502
2	-1.464	1.451	0.107	-0.092	0.573		-1.892	2	0.8
3	-1.038	-0.717	-1.379	2.01	-0.112		1.468	3	-1.376
4	0.564	-0.695	1.207	1.029	1.409		-1.02	4	-0.406
5	-0.509	-0.272	1.144	1.774	-1.407		-0.817	5	-1.180
6	1.223	-0.101	1.49	-0.994	0.758		-0.206	6	-0.116
7	-1.241	0.441	1.66	-0.04	0.995		0.317	7	-0.951
8	1.302	-1.259	0.757	-1.179	0.153		0.615	8	0.782
9	0.181	1.656	0.068	0.194	-1.565		1.03	9	-0.546
10	1.245	0.241	-1.671	-1.322	0.591		-1.39	10	-1.082
11	1.608	1.067	-0.303	-1.064	-0.6015		-1.854	11	-0.399
12	-0.753	-0.539	-1.498	1.033	1.297		-2.301	12	-0.07
								Bias	-0.816
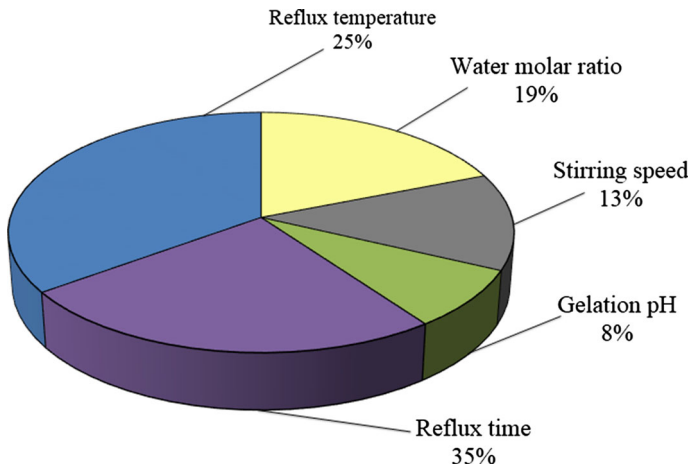
Fig. 9 Relative importance (%) of the input synthesis variables on the k_{ap} values of the AR27 removal

nanoparticles in the removal of AR27 was successfully simulated by using neural network modeling, and there was good agreement between the results predicted by the ANN model and the experimental results with a correlation coefficient (R^2) of 0.9655 and MSE of 0.00148. The sensitivity analysis showed that reflux time and reflux temperature variables with a relative importance of 35 and 25 %, respectively, have larger effects on the photocatalytic activity of TiO$_2$, and gelation pH has the lowest influence on the photocatalytic activity of TiO$_2$.

References

1. Y. Liu, X. Wang, F. Yang, X. Yang, Microporous Mesoporous Mater. **114**, 431 (2008)
2. A.M. More, J.L. Gunjakar, C.D. Lokhande, Sens. Actuat. B **129**, 671 (2008)
3. M.I. Mejía, J.M. Marín, G. Restrepo, C. Pulgarín, E. Mielczarski, J. Mielczarski, Y. Arroyo, J.-C. Lavanchy, J. Kiwi, Appl. Catal. B **91**, 481 (2009)
4. V.P.S. Perera, P.V.V. Jayaweera, P.K.D.D.P. Pitigala, P.K.M.B. Andaranayake, G. Hastings, A.G.U. Perera, K. Tennakone, Synth. Met. **143**, 283 (2004)
5. Y.-H. Hsien, C.-F. Chang, Y.-H. Chen, S. Cheng, Appl. Catal. B **31**, 241 (2001)
6. M.A. Behnajady, H. Eskandarloo, N. Modirshahla, M. Shokri, Dig. J. Nanomater. Biostruct. **6**, 1887 (2011)
7. Y. Zhao, C. Li, X. Liu, F. Gu, H.L. Du, L. Shi, Appl. Catal. B **79**, 208 (2008)
8. T. Sugimoto, X. Zhou, A. Muramatsu, J. Colloid Interface Sci. **252**, 339 (2002)
9. X. Wang, T–.T. Lim, Appl. Catal. B **100**, 355 (2010)
10. T. Maekawa, K. Kurosaki, T. Tanaka, S. Yamanaka, Surf. Coat. Technol. **202**, 3067 (2008)
11. N.R. de Tacconi, C.R. Chenthamarakshan, G. Yogeeswaran, A. Watcharenwong, R.S. de Zoysa, A.N. Basit, K. Rajeshwar, J. Phys. Chem. B **110**, 25347 (2006)
12. C. Shifu, C. Lei, G. Shen, C. Gengyu, Chem. Phys. Lett. **413**, 404 (2005)
13. D.S. Kim, S.-Y. Kwak, Appl. Catal. A Gen. **323**, 110 (2007)
14. S.K. Sharma, M. Vishwas, K.N. Rao, S. Mohan, D.S. Reddy, K.V.A. Gowda, J. Alloys Compd. **471**, 244 (2009)

15. M.A. Behnajady, H. Eskandarloo, Res. Chem. Intermed. (2012). doi:10.1007/s11164-013-1327-5
16. F. Ghanbary, N. Modirshahla, M. Khosravi, M.A. Behnajady, J. Environ. Sci. **24**, 750 (2012)
17. E.S. Elmolla, M. Chaudhuri, M.M. Eltoukhy, J. Hazard. Mater. **179**, 127 (2010)
18. A.R. Khataee, O. Mirzajani, Desalination **251**, 64 (2010)
19. A. Duran, J.M. Monteagudo, M. Mohedano, Appl. Catal. B **65**, 127 (2006)
20. M.A. Behnajady, H. Eskandarloo, N. Modirshahla, M. Shokri, Desalination **278**, 10 (2011)
21. V.K. Pareek, M.P. Brungs, A.A. Adesina, R. Sharma, J. Photochem. Photobiol. A **149**, 139 (2002)
22. D. Salari, N. Daneshvar, F. Aghazadeh, A.R. Khataee, J. Hazard. Mater. **125**, 205 (2005)
23. M.B. Kasiri, H. Aleboyeh, A. Aleboyeh, Environ. Sci. Technol. **42**, 7970 (2008)
24. A. Aleboyeh, M.B. Kasiri, M.E. Olya, H. Aleboyeh, Dyes Pigment **77**, 288 (2008)
25. Y. Bessekhouad, D. Robert, J.V. Weber, J. Photochem. Photobiol. A **157**, 47 (2003)
26. M.A. Behnajady, H. Eskandarloo, N. Modirshahla, M. Shokri, Photochem. Photobiol. **87**, 1002 (2011)
27. A. Bandgar, S. Sabale, S.H. Pawar, Ceram. Int. **38**, 1905 (2012)
28. L. Ge, M. Xu, M. Sun, H. Fang, J. Sol-Gel Sci. Technol. **38**, 47 (2006)
29. N. Barati, M.A. Faghihi Sani, H. Ghasemi, Z. Sadeghian, S.M.M. Mirhoseini, Appl. Surf. Sci. **255**, 8328 (2009)
30. D. Zhang, L. Qi, J. Ma, H. Cheng, J. Mater. Chem. **12**, 3677 (2002)
31. W. Qiu, C.-J. Ren, Q. Wei, M.-C. Gong, Y.-Z. Hou, Y.-Q. Chen, Acta Phys. Chim. Sin. **27**, 1487 (2011)
32. N.-G. Park, G. Schlichthörl, J. Van de Lagemaat, H.M. Cheong, A. Mascarenhas, A.J. Frank, J. Phys. Chem. B **103**, 3308 (1999)
33. J.G. Yu, Y.R. Su, B. Cheng, Adv. Funct. Mater. **17**, 1984 (2007)
34. K. Panpae, S. Angkaew, C. Sritara, C. Ngernsuttichaiporn, Kasetsart J. (Nat. Sci.) **41**, 178 (2007)
35. S. Sathyamoorthy, M.J. Hounslow, G.D. Moggridge, J. Cryst. Growth **223**, 225 (2001)
36. A.R. Soleymani, J. Saien, H. Bayat, Chem. Eng. J. **170**, 29 (2011)
37. G.D. Garson, AI Expert **6**, 47 (1991)